Nonparametric stochastic modeling of structural dynamic systems with uncertain boundary conditions

M. P. Mignolet, Christian Soize

M. P. Mignolet, C. Soize, Nonparametric stochastic modeling of structural dynamic systems with uncertain boundary conditions. AIAA Conference, Schaumburg (Chicago), Illinois, USA, 7-10 April 2008.

NONPARAMETRIC STOCHASTIC MODELING OF STRUCTURES WITH UNCERTAIN BOUNDARY CONDITIONS AND UNCERTAIN COUPLING BETWEEN SUBSTRUCTURES

Marc P. Mignolet*
Arizona State University, Tempe, AZ 85287-6106, USA
Christian Soize‡
Universite Paris-Est, 77454 Marne-la-Vallee, France

ABSTRACT

The focus of this investigation is on the formulation and validation of a novel approach for the inclusion of uncertainty in the modeling of the boundary conditions of linear structures and of the coupling between linear substructures. First, a mean structural dynamic model that includes boundary condition/coupling flexibility is obtained using classical substructuring concepts. The application of the nonparametric stochastic modeling approach to this mean model is next described and thus permits the consideration of both model and parameter uncertainty. Finally, a dedicated identification procedure is proposed to estimate the two parameters of this stochastic model, i.e. the mean boundary condition/coupling flexibility and the overall level of uncertainty.

INTRODUCTION

Significant efforts have been focused in the last decade or so on the modeling and consideration of uncertainty in the properties of structural dynamic systems. In fact, two types of uncertainty have been recognized. Parameter uncertainty refers to a lack of knowledge of the exact values of the parameters of the physical and/or computational model, e.g. of the Young's modulus. Model uncertainty on the other hand relates to discrepancies between the physical structure and its model that arise in the modeling effort, e.g. in the representation of the connection between two parts by rivets, spotwelds, etc. The nonparametric stochastic modeling approach provides a convenient strategy for the consideration of both types of uncertainties by operating at the level of the reduced order model of the structural dynamic system.

Notorious sources of uncertainty in structures are the boundary conditions (especially the clamped ones) and the coupling between substructures. In fact, both lead to significant model and parameter uncertainties. Consider for example the clamped boundary condition although a similar discussion can be carried for other boundary conditions and for the coupling between substructures. A first modeling strategy of a physical clamped boundary condition is in terms of its mathematical counterpart, i.e. zero displacements and slopes. This approach however completely neglects the unavoidable flexibility of the support and clamp and thus leads to an overestimation of the natural frequencies. More refined models have also been proposed that do account for this flexibility through the introduction of stiffnesses at the interface between the structure and its support considered rigid. However, the determination of the corresponding boundary stiffness matrix is a particularly challenging task due to the large number of components that it would involve. This issue has in turn been resolved by selecting a particular form for the stiffness matrix, e.g. in terms of the stiffness matrix of the structure at its boundary, with one or several parameters that are identifiable from a few experiments. Nevertheless, this approach leads only to a *model* of the physical situation and does not include other factors such as possible contact nonlinearity, friction, etc. Accordingly, model uncertainty is fully expected in this ad hoc representation of the boundary condition.

Parameter uncertainty must also be considered in the boundary condition modeling to simulate the variability in the dynamic response (e.g. natural frequencies, mode shapes, etc.) of a particular structure and support that originates most notoriously from the level of normal force applied at the clamp but also from the state of surface/wear of the structure at its boundary and of the clamp, etc.

In this light, the focus of this paper is on the

* Professor, Department of Mechanical and Aerospace Engineering, Associate Fellow, AIAA.
‡ Professor, Laboratoire Modelisation et Simulation Multi Echelle.

formulation and validation of a novel procedure for the *explicit* consideration of model and parameter uncertainty in both boundary conditions and coupling between substructures. Further, this treatment will be conducted within the framework of the nonparametric approach [1,2]. Accordingly, this approach is first briefly reviewed.

NONPARAMETRIC STOCHASTIC MODELING OF UNCERTAINTY

The fundamental problem of the nonparametric approach is the simulation of random symmetric positive definite real matrices $\underline{\underline{A}}$ such as the mass, damping, and/or stiffness matrices of linear modal models. To achieve this effort, it is necessary to specify which (joint) statistical distribution of their elements A_{ij} should be adopted. In this regard, it will first be assumed that the mean of the random matrix $\underline{\underline{A}}$ is known as $\overline{\underline{\underline{A}}}$, i.e. $E\left[\underline{\underline{A}}\right]=\overline{\underline{\underline{A}}}$ where $E[.]$ denotes the operation of mathematical expectation. If, as discussed above, the fixed modes used to represent the motion of the uncertain structures are those associated with the mean structural model (also referred to as the design conditions model) and are mass normalized, then the mean of the random mass and stiffness matrices are the identity matrix and the diagonal matrix of the squared natural frequencies, respectively. Further, if the mean model does not exhibit any rigid body mode (i.e. $\overline{\underline{\underline{A}}}$ is strictly positive definite), then it is also expected that the random matrices $\underline{\underline{A}}$ will share the same property (note that the extension of the methodology to mean models exhibiting rigid body modes has been accomplished in [3]). This condition is equivalent to the existence of a flat zero at zero of the probability density function of the eigenvalues of $\underline{\underline{A}}$. Finally, it will be assumed that only a single measure of the variability of the matrices $\underline{\underline{A}}$ is available, e.g. the standard deviation of the lowest eigenvalue of $\underline{\underline{A}}$ (the extension of the methodology to account for multiple known measures of variability has been accomplished in [4]).

Even with the above assumptions (known mean model, nonsingularity of $\underline{\underline{A}}$, and known measure of variability), there is a broad set of statistical distributions of the elements A_{ij} that could be selected. Among those, it would be particularly desirable to select the one that places particular emphasis on "larger" deviations from the mean value, a desirable feature to assess, in a limited Monte Carlo study, the aeroelastic robustness of a design to uncertainty. As discussed in references [1-4], this property is achieved by the distribution of the elements A_{ij} that achieves the *maximum of the statistical entropy* under the stated constraints of symmetry, positive definiteness, known mean model, nonsingularity of $\underline{\underline{A}}$, and known measure of variability. This maximum is satisfied (see [1-4]) when the matrices $\underline{\underline{A}}$ are generated as

$$\underline{\underline{A}} = \overline{\underline{\underline{L}}}\ \underline{\underline{H}}\,\underline{\underline{H}}^T\,\overline{\underline{\underline{L}}}^T \qquad (1)$$

where $\overline{\underline{\underline{L}}}$ is any decomposition, e.g. Cholesky, of $\overline{\underline{\underline{A}}}$, i.e. satisfying $\overline{\underline{\underline{A}}} = \overline{\underline{\underline{L}}}\,\overline{\underline{\underline{L}}}^T$. Further, $\underline{\underline{H}}$ denotes a lower triangular random matrix the elements of which are all statistically independent of each other. Moreover, the probability density functions of the diagonal (H_{ii}) and off-diagonal elements (H_{il}) are

$$p_{H_{ii}}(h) = C_{ii}\, h^{p(i)} \exp\left[-\mu h^2\right]\ ,\ h \geq 0 \qquad (2)$$

and

$$p_{H_{il}}(h) = C_{il}\ \exp\left[-\mu h^2\right]\ ,\ h \geq 0\ ,\ i \neq l \qquad (3)$$

where

$$p(i) = n - i + 2\lambda - 1 \qquad \mu = \frac{n + 2\lambda - 1}{2} \qquad (4)$$

$$C_{ii} = \frac{2\mu^{[p(i)+1]/2}}{\Gamma\left((p(i)+1)/2\right)} \qquad C_{il} = \sqrt{\frac{\mu}{\pi}} \qquad (5)$$

In these equations, n denotes the size of the matrices $\underline{\underline{A}}$, i.e. the number of modes retained, and $\Gamma(.)$ denotes the Gamma function. In fact, it is readily seen that (see also Fig. 1):

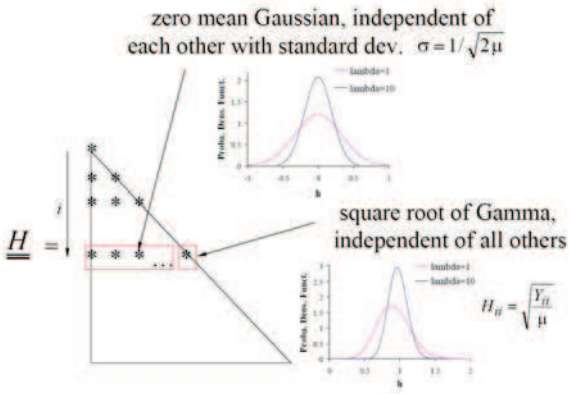

Figure 1: Structure of the random $\underline{\underline{H}}$ matrices (figures for n=8, i=2, and λ=1 and 10)

In the above equations, the parameter $\lambda > 0$ is the free parameter of the statistical distribution of the random matrices $\underline{\underline{H}}$ and $\underline{\underline{A}}$ and can be evaluated to meet any given information about their variability. In the ensuing examples, the parameter λ will be determined to yield a specified value of the overall measure of uncertainty δ defined as

$$\delta^2 = \frac{1}{n} E\left[\left\| \underline{\underline{H}}\,\underline{\underline{H}}^T - \underline{\underline{I}} \right\|_F^2 \right] = \frac{n+1}{n+2\lambda-1} \qquad (6)$$

where $\underline{\underline{I}}$ denotes the identity matrix, $\| \ \|_F$ denotes the Frobenius norm of a matrix, and $E[\ ]$ designates the operation of mathematical expectation. This condition, coupled with Eqs (1)-(5), provides a complete scheme for the generation of random symmetric positive definite matrices $\underline{\underline{A}}$.

UNCERTAIN CLAMPED BOUNDARY CONDITIONS

Modeling strategy

A perfect clamped boundary cannot exhibit any uncertainty as the displacements and slopes are exactly set to zero. The physical problem which is thus modeled is one in which there is flexibility at the boundary and it is that flexibility which is uncertain. The first step in the present effort is thus to replace the perfect clamped boundary condition by an "imperfect"/flexible one which is represented by a distribution of springs (both linear and torsional), see Fig. 2. This discussion will be carried out first in the absence of uncertainty in the boundary conditions which will then be introduced in the second step.

Assuming that the modeling of the structure is accomplished with finite elements, the next step is to proceed with a partitioning of the degrees-of-freedom of the structure with flexible boundary conditions in terms of internal (I) and boundary (B) degrees-of-freedom. Accordingly, the stiffness matrix of the structure may be expressed as

$$\underline{\underline{K}}_{phys} = \overline{\underline{\underline{K}}}_{phys} + \hat{\underline{\underline{K}}}_{phys} \qquad (7)$$

where, in partitioned form,

$$\overline{\underline{\underline{K}}}_{phys} = \begin{bmatrix} \overline{\underline{\underline{K}}}^{II}_{phys} & \overline{\underline{\underline{K}}}^{IB}_{phys} \\ \overline{\underline{\underline{K}}}^{BI}_{phys} & \overline{\underline{\underline{K}}}^{BB}_{phys} \end{bmatrix}$$

and

$$\hat{\underline{\underline{K}}}_{phys} = \begin{bmatrix} \underline{\underline{0}} & \underline{\underline{0}} \\ \underline{\underline{0}} & \hat{\underline{\underline{K}}}^{BB}_{phys} \end{bmatrix}. \qquad (8)$$

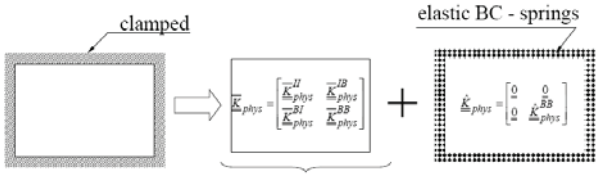

Figure 2. Transformation of the perfect clamped boundary condition into a flexible boundary condition and separation of the domains.

Note in this decomposition that $\overline{\underline{\underline{K}}}_{phys}$ is the stiffness matrix of the free-free structure. Assuming that the boundary is massless, one obtains similarly

$$\underline{\underline{M}}_{phys} = \overline{\underline{\underline{M}}}_{phys} \qquad (9)$$

with

$$\overline{\underline{\underline{M}}}_{phys} = \begin{bmatrix} \overline{\underline{\underline{M}}}^{II}_{phys} & \overline{\underline{\underline{M}}}^{IB}_{phys} \\ \overline{\underline{\underline{M}}}^{BI}_{phys} & \overline{\underline{\underline{M}}}^{BB}_{phys} \end{bmatrix}. \qquad (10)$$

A first reduced order model of the structure with flexible boundary conditions can be derived by proceeding with a Craig-Bampton approach, i.e. by expressing the internal ($\underline{X}^I_{phys}$) and boundary ($\underline{X}^B_{phys}$) degrees-of-freedom as

$$\underline{X}^I_{phys} = \underline{\underline{\Phi}}\,\underline{q} + \underline{\underline{\Xi}}\,\underline{Y} \qquad (11)$$

and

$$\underline{X}^B_{phys} = \underline{Y} \qquad (12)$$

where $\underline{\underline{\Phi}}$ denotes the modal matrix of p selected modes of the clamped structure, i.e. $\underline{\underline{\Phi}} = \left[\underline{\phi}_1 \ \underline{\phi}_2 \ \mathrm{K} \ \underline{\phi}_p \right]$, where

$$\overline{\underline{\underline{K}}}^{II}_{phys}\,\underline{\phi}_j = \omega^2_{C,j}\,\overline{\underline{\underline{M}}}^{II}_{phys}\,\underline{\phi}_j . \qquad (13)$$

Further, in Eq. (11), the symbol $\underline{\underline{\Xi}}$ denotes the matrix of constraint modes

$$\underline{\underline{\Xi}} = -\left(\overline{\underline{\underline{K}}}^{II}_{phys} \right)^{-1} \overline{\underline{\underline{K}}}^{IB}_{phys} . \qquad (14)$$

Finally, the vector $\underline{q}$ denotes the generalized coordinates of the modes of the clamped structure.

The reduction of variables, from $\left(\underline{X}^I_{phys}, \underline{X}^B_{phys} \right)$ to $\left(\underline{q}, \underline{Y} \right)$, is accompanied by the matrix

$$\underline{\underline{T}}_1 = \begin{bmatrix} \underline{\underline{\Phi}} & \underline{\underline{\Xi}} \\ \underline{\underline{0}} & \underline{\underline{I}} \end{bmatrix} \qquad (15)$$

and thus, the stiffness and mass matrices of the free-free structure associated with the variables $\left(\underline{q}, \underline{Y} \right)$ are

$$\underline{\underline{K}}_{CB} = \underline{\underline{T}}_1^T\,\overline{\underline{\underline{K}}}_{phys}\,\underline{\underline{T}}_1 = \begin{bmatrix} \underline{\underline{K}}^{qq}_{CB} & \underline{\underline{K}}^{qY}_{CB} \\ \underline{\underline{K}}^{Yq}_{CB} & \underline{\underline{K}}^{YY}_{CB} \end{bmatrix} \qquad (16)$$

and

$$\underline{\underline{M}}_{CB} = \underline{\underline{T}}_1^T \, \overline{\underline{\underline{M}}}_{phys} \, \underline{\underline{T}}_1 = \begin{bmatrix} \underline{\underline{M}}_{CB}^{qq} & \underline{\underline{M}}_{CB}^{qY} \\ \underline{\underline{M}}_{CB}^{Yq} & \underline{\underline{M}}_{CB}^{YY} \end{bmatrix}. \quad (17)$$

Since the reduced order model is built on the modal matrix $\underline{\underline{\Phi}}$, the matrices $\underline{\underline{K}}_{CB}^{qq}$ and $\underline{\underline{M}}_{CB}^{qq}$ are diagonal, and more specifically with nonzero elements equal to the natural frequencies and 1 if the modes $\underline{\phi}_j$ have been normalized with respect to the mass matrix $\overline{\underline{\underline{M}}}_{phys}^{II}$.

The reduced order model of Eq. (11) and (12) is in fact "mixed" as it contains both modal coordinates (for the internal degrees-of-freedom) and physical coordinates (for the boundary degrees-of-freedom). A "fully" reduced order model can be developed by expressing the physical boundary degrees-of-freedom as

$$\underline{Y} = \underline{\underline{\Psi}} \, \underline{u} \quad (18)$$

where $\underline{\underline{\Psi}} = \left[\underline{\psi}_1 \, \underline{\psi}_2 \, \mathrm{K} \, \underline{\psi}_r \right]$ and the vectors $\underline{\psi}_j$ are an appropriate basis for the representation of the physical boundary degrees-of-freedom, for instance the eigenvectors corresponding to $\underline{\underline{K}}_{CB}^{YY}$ and $\underline{\underline{M}}_{CB}^{YY}$. That is,

$$\underline{\underline{K}}_{CB}^{YY} \, \underline{\psi}_j = \lambda_j \, \underline{\underline{M}}_{CB}^{YY} \, \underline{\psi}_j . \quad (19)$$

This second reduction of degrees-of-freedom is accompanied by the matrix

$$\underline{\underline{T}}_2 = \begin{bmatrix} \underline{\underline{I}} & \underline{\underline{0}} \\ \underline{\underline{0}} & \underline{\underline{\Psi}} \end{bmatrix} \quad (20)$$

and thus, the stiffness and mass matrices of the free-free structure associated with the variables $\left(\underline{q}, \underline{u}\right)$ are

$$\overline{\underline{\underline{K}}}_{ROM} = \underline{\underline{T}}_2^T \, \underline{\underline{K}}_{CB} \, \underline{\underline{T}}_2 = \begin{bmatrix} \overline{\underline{\underline{K}}}_{ROM}^{qq} & \overline{\underline{\underline{K}}}_{ROM}^{qu} \\ \overline{\underline{\underline{K}}}_{ROM}^{uq} & \overline{\underline{\underline{K}}}_{ROM}^{uu} \end{bmatrix} \quad (21)$$

and

$$\overline{\underline{\underline{M}}}_{ROM} = \underline{\underline{T}}_2^T \, \underline{\underline{M}}_{CB} \, \underline{\underline{T}}_2 = \begin{bmatrix} \overline{\underline{\underline{M}}}_{ROM}^{qq} & \overline{\underline{\underline{M}}}_{ROM}^{qu} \\ \overline{\underline{\underline{M}}}_{ROM}^{uq} & \overline{\underline{\underline{M}}}_{ROM}^{uu} \end{bmatrix}. \quad (22)$$

The above discussion focused solely on the free-free structure but the consideration of its flexible boundary counterpart is accomplished simply through the addition of the finite boundary stiffness matrix $\hat{\underline{\underline{K}}}_{phys}$, see Eq. (7) and (8). In practical situations, this matrix is generally not known which in fact is why a perfect clamped boundary condition is often introduced. The next level of complexity, which will be adopted here, is to relate $\hat{\underline{\underline{K}}}_{phys}$ to the boundary-boundary partition of the stiffness matrix of the free-free structure. This relation is most conveniently achieved directly in the reduced order model variables, i.e. by specifying

$$\hat{\underline{\underline{K}}}_{ROM}^{uu} = k \, \underline{\underline{\Psi}}^T \, \overline{\underline{\underline{K}}}_{phys}^{BB} \, \underline{\underline{\Psi}} \quad (23)$$

where

$$\hat{\underline{\underline{K}}}_{ROM} = \underline{\underline{T}}_2^T \, \underline{\underline{T}}_1^T \, \hat{\underline{\underline{K}}}_{phys} \, \underline{\underline{T}}_1 \, \underline{\underline{T}}_2 = \begin{bmatrix} 0 & 0 \\ 0 & \hat{\underline{\underline{K}}}_{ROM}^{uu} \end{bmatrix} \quad (24)$$

is the stiffness matrix of the boundary conditions in the reduced order variables $\left(\underline{q}, \underline{u}\right)$. The parameter k in Eq. (23) is a scalar that constitutes a parameter of the boundary condition modeling.

Combining the preceding results, it is found that the overall ROM stiffness matrix is

$$\underline{\underline{K}}_{ROM} = \overline{\underline{\underline{K}}}_{ROM} + \hat{\underline{\underline{K}}}_{ROM} = \begin{bmatrix} \overline{\underline{\underline{K}}}_{ROM}^{qq} & \overline{\underline{\underline{K}}}_{ROM}^{qu} \\ \overline{\underline{\underline{K}}}_{ROM}^{uq} & \overline{\underline{\underline{K}}}_{ROM}^{uu} + k \, \hat{\underline{\underline{K}}}_{ROM}^{uu} \end{bmatrix} . \quad (25)$$

The determination of the natural frequencies $\omega_{f,j}$ and mode shapes $\underline{\varphi}_j$ of the flexible boundary structure is achieved by solving the eigenvalue problem

$$\underline{\underline{K}}_{ROM} \, \underline{\varphi}_j = \omega_{f,j}^2 \, \overline{\underline{\underline{M}}}_{ROM} \, \underline{\varphi}_j . \quad (26)$$

The consideration of uncertainty on the free-free structure is easily performed from Eq. (25) through the nonparametric approach [1-4]. Specifically, if the free-free structure is uncertain, a random reduced order stiffness matrix $\underline{\underline{\underline{K}}}_{ROM}$ can be obtained as $\underline{\underline{\underline{K}}}_{ROM} = \overline{\underline{\underline{L}}}_{ROM} \, \underline{\underline{\underline{H}}} \, \underline{\underline{\underline{H}}}^T \, \overline{\underline{\underline{L}}}_{ROM}^T + \hat{\underline{\underline{K}}}_{ROM}$ where $\overline{\underline{\underline{L}}}_{ROM}$ is the Cholesky decomposition of $\overline{\underline{\underline{K}}}_{ROM}$, i.e. the lower triangular matrix satisfying the equation $\overline{\underline{\underline{K}}}_{ROM} = \overline{\underline{\underline{L}}}_{ROM} \, \overline{\underline{\underline{L}}}_{ROM}^T$. Further, $\underline{\underline{\underline{H}}}$ denotes the random matrix of Eqs (2)-(5), see also Fig. 1. Uncertainty in boundary conditions alone is introduced similarly by replacing the mean model matrix $k \, \hat{\underline{\underline{K}}}_{ROM}^{uu}$ by $k \, \underline{\underline{\underline{K}}}_{ROM}^{uu} = k \, \overline{\underline{\underline{L}}}_{ROM}^{uu} \, \underline{\underline{\underline{H}}}^{uu} \left(\underline{\underline{\underline{H}}}^{uu} \right)^T \left(\overline{\underline{\underline{L}}}_{ROM}^{uu} \right)^T$ where $\overline{\underline{\underline{L}}}_{ROM}^{uu}$ is the Cholesky decomposition of $\overline{\underline{\underline{K}}}_{ROM}^{uu} = \overline{\underline{\underline{L}}}_{ROM}^{uu} \left(\overline{\underline{\underline{L}}}_{ROM}^{uu} \right)^T$ and $\underline{\underline{\underline{H}}}^{uu}$ is another random matrix also defined by Eqs (2)-(5), see also Fig. 1.

Examples of Application

To demonstrate the process discussed above and clarify the effects of the parameters k and δ, an aluminum clamed plate of dimensions 0.3556mx0.254mx0.001m

was considered. The material properties of aluminum were selected as E = 70,000MPa, ν=0.30, ρ=2700kg/m^3. A first set of computations was carried out without uncertainty to analyze the mean model and in particular the relation between natural frequencies and the value of k which is plotted in Fig. 3 for the first seven natural frequencies. The values in the

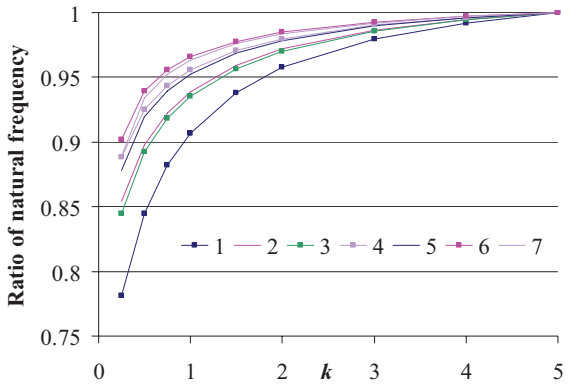

Figure 3. Ratio of the first seven natural frequencies to their k=∞ counterparts as function of k.

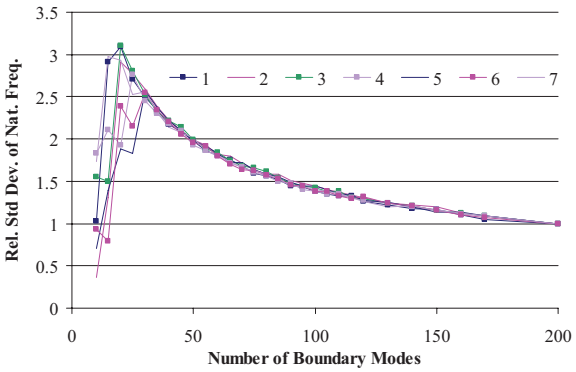

Figure 4. Standard deviation of the 7 lowest natural frequencies divided by the asymptotic value, as a function of the number of boundary modes, k=0.75, δ=0.1. Ratio of the first seven natural frequencies to their k=∞ counterparts as function of k.

ordinate correspond to the natural frequencies for a finite value of k divided by their k=∞ counterpart. As expected, the natural frequencies converge monotonically to those of the perfectly clamped plate. It was next desired to assess the convergence of the model prediction with increasing number of boundary modes $\underline{\psi}_j$. Both the natural frequencies and boundary energy were investigated and in both cases it was found that the mean value converged must faster than the standard deviation. Further, the standard deviations of the boundary energy and the natural frequencies

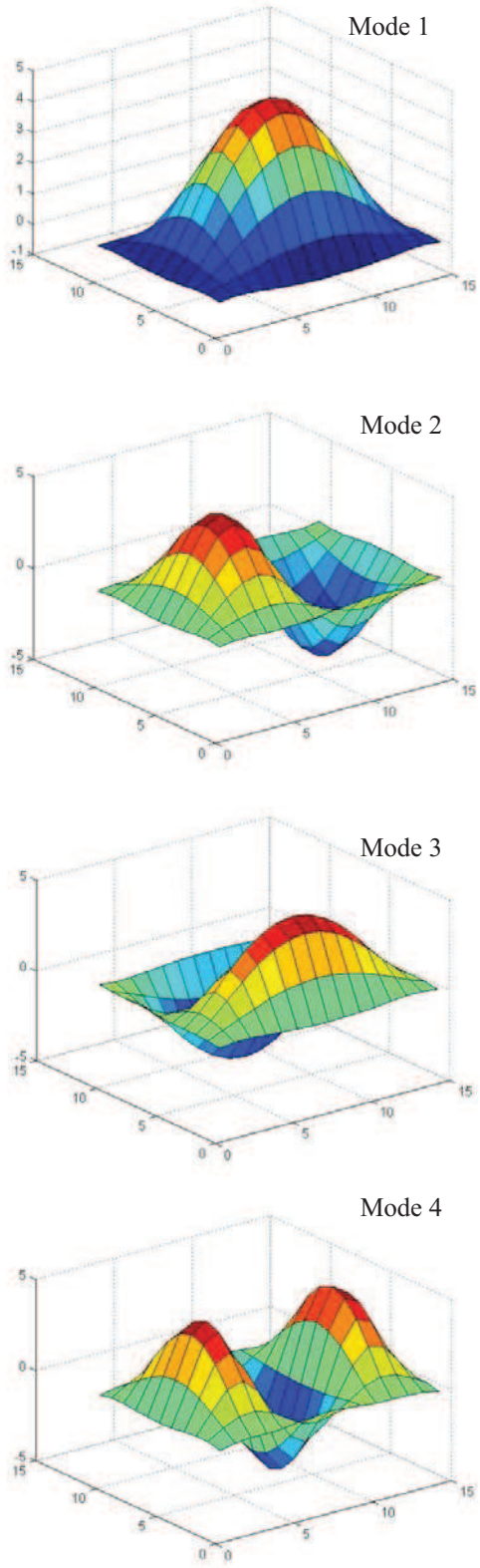

Figure 5. First four modes of the flexible boundary plate, k =0.75, 120 boundary modes, 10 clamped modes

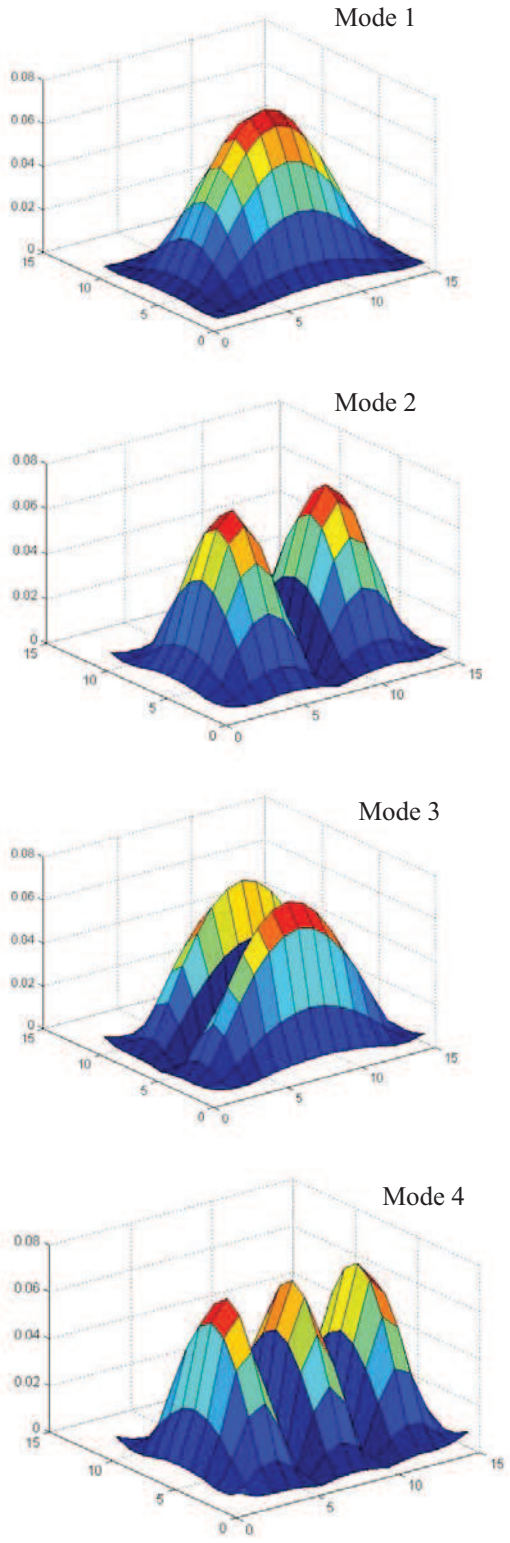

Figure 6. Standard deviation of modal values, first 4 modes, k =0.75,120 boundary modes, 10 clamped modes, and δ=0.1.

exhibited a very similar behavior, see Fig. 4 for the natural frequencies. It is seen in particular that the convergence is rather slow but appears to be the same for all natural frequencies.

The properties of the mode shapes were also investigated. Shown in Fig. 5 are the first 4 modes of the flexible boundary condition plate with k=0.75 and note the slight displacements and rotations at the boundary. The variation of the modal properties with uncertainty was also analyzed, e.g. see Fig. 6 for the standard deviation of the modal values for the first 4 modes. Note the strong similarity between the modes and their standard deviations.

The model of uncertain boundary conditions developed in the previous section is a 2 parameter model as it involves the coefficient k of Eq. (23) and the uncertainty measure δ of Eq. (6), and it was accordingly desired to assess the joint effect of these 2 parameters. Shown in Fig. 7 are the coefficients of variations of the

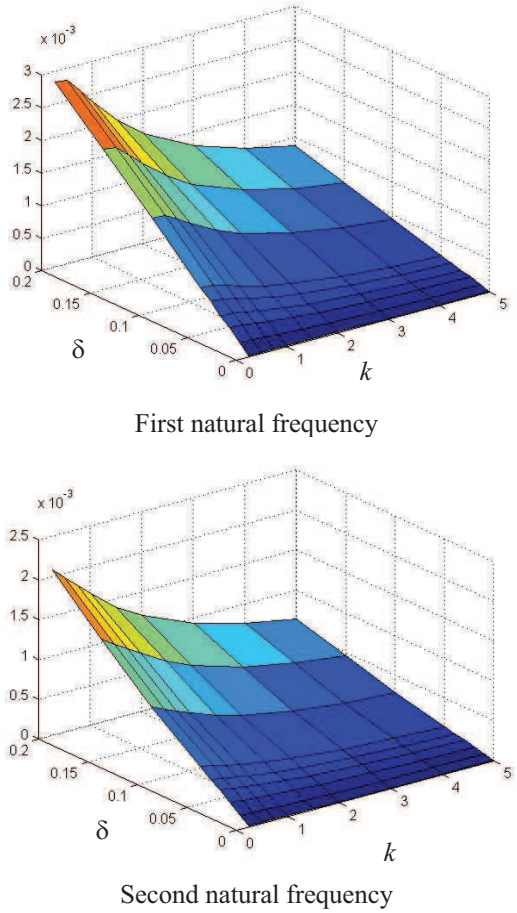

Figure 7. Coefficients of variation of the first two natural frequency vs. k and δ, 120 boundary modes, 10 clamped modes.

first two natural frequencies, as functions of k and δ. These plots do exhibit expected behaviors. the coefficients of variations all grow as a function of the uncertainty measure for all values of k. Second, these coefficients of variations are also monotonically decreasing functions of k as might be expected since the limit $k \to \infty$ should recover the perfectly clamped plate for which the natural frequencies do not exhibit any variability.

To complete the modeling process, it remains to formulate an identification strategy of the two parameters of the boundary conditions uncertainty model, i.e. k and δ. It is proposed here to focus on metrics that relate to the motions at the boundary to avoid the interference of uncertainty on the rest of the structure. More specifically, consider the boundary condition "energy" term E_{BC} defined as

$$E_{BC} = \left(\underline{X}^B_{phys}\right)^T A_{BC}\, \underline{X}^B_{phys} \qquad (27)$$

where A_{BC} is a specified positive definite matrix. It is then desired to assess the existence of strong correlation between some properties of E_{BC} and the parameters k and δ. Shown in Fig. 8 are the mean and coefficient of variation of E_{BC} for the first random

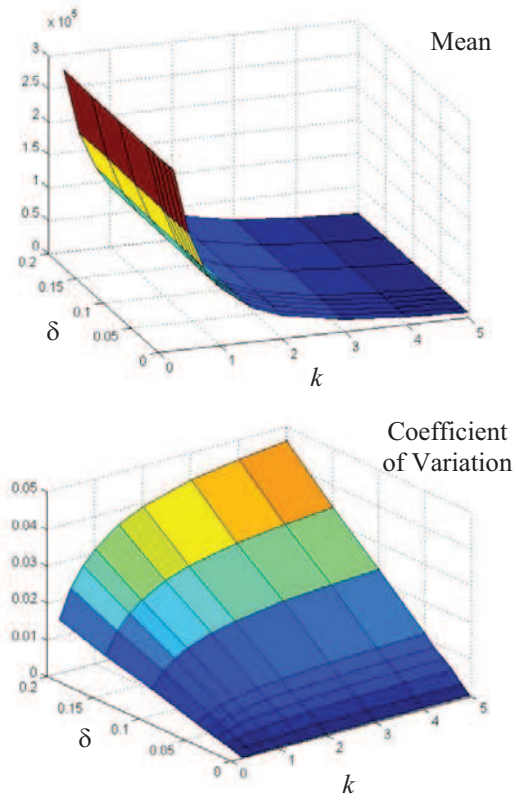

Figure 8. Mean and coefficient of variation of E_{BC}, first mode deformations, vs. k and δ, 120 boundary modes, 10 clamped modes.

mode with A_{BC} arbitrarily chosen as a diagonal matrix with elements equal to 1 on translations and 10 on rotations. It is clearly seen from these figures that the mean of E_{BC} provides an unambiguous estimation of k while the variance of E_{BC} has a clear dependence on δ. Thus, the knowledge of the first two moments of the quantity E_{BC} provides straightforward estimates of k and δ.

The analysis of the effects of uncertainty in the boundary conditions can extend further than the natural frequencies and mode shapes of the structure, e.g. to the flutter boundary. To exemplify this application, the Goland wing of Fig. 9 (see Table 1 for natural frequencies) was considered and its flutter boundary was determined for M_∞=0.7 using ZAERO and a 20 mode model (see [5,6] for related investigations). An analysis of the fully clamped wing demonstrated that flutter occurs at 752.87 ft/s with a frequency of 1.966Hz.

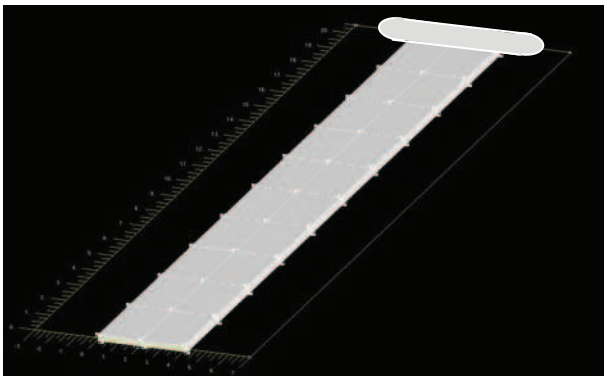

Figure 9. The Goland wing model.

Mode #	Nat. Freq. (Hz)	Mode #	Nat. Freq. (Hz)
1	1.690	6	16.260
2	3.051	7	22.845
3	9.172	8	26.318
4	10.834	9	29.183
5	11.258		

Table 1. Natural frequencies of the mean Goland wing

It was next desired to assess the variations of the flutter speed and flutter frequency that would result from uncertainty in the clamped boundary condition. To this end, the formulation of the previous section was applied with a value k = 20 with 12 cantilevered modes and 8 boundary modes. These parameter selections led to first and second natural frequencies without uncertainty equal to 98.8% and 99.4% of their fully clamped counterparts.

Next, uncertainty was introduced using the nonparametric approach and the value δ=0.6 was chosen; it leads to coefficients of variation of the first and second natural frequencies of 0.28% and 0.14%, respectively. Next, an ensemble of 300 uncertain wings were simulated and their flutter boundary was determined using ZAERO for M_∞=0.7 with a 20 mode model based on the mean wing with flexible boundary conditions. Shown in Fig. 10 are the first and second natural frequencies of these wings (Fig. 10(a)) and their corresponding matched point flutter boundaries (Fig. (10b)).

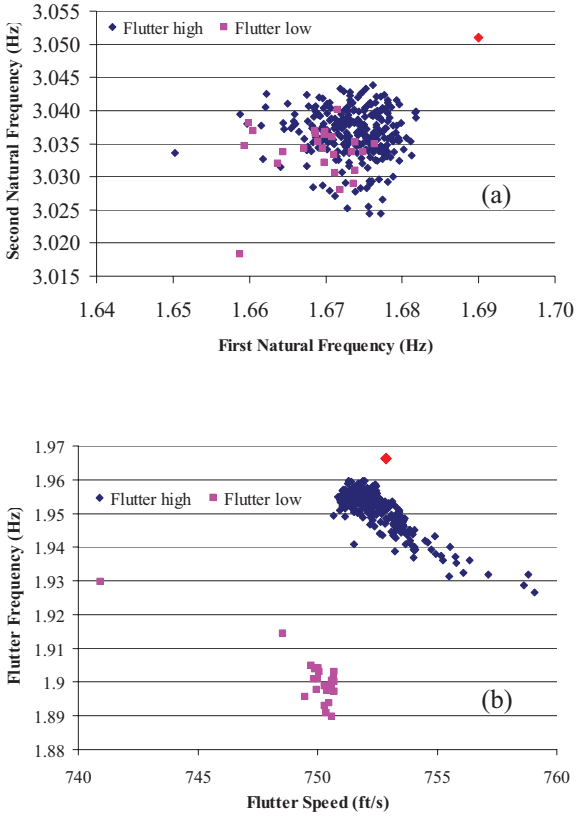

Figure 10. Shotgun plot of (a) first and second natural frequencies, (b) flutter frequency vs. flutter speed, random boundary conditions. The red triangle denotes the design conditions (fully clamped wing).

It must be noted from Fig. 10 that the variations in flutter frequency and especially flutter speed are much larger than the corresponding variations of the natural frequencies. Note finally that the 300 flutter cases can be separated into two groups exhibiting either high or low flutter speed and frequency (see Fig. 10(b)). The probability density functions of Fig. 11 highlight these two findings.

These observations are consistent with the results of [6] which demonstrated the high sensitivity, both quantitatively and qualitatively, of the Goland wing flutter boundary to structural uncertainty.

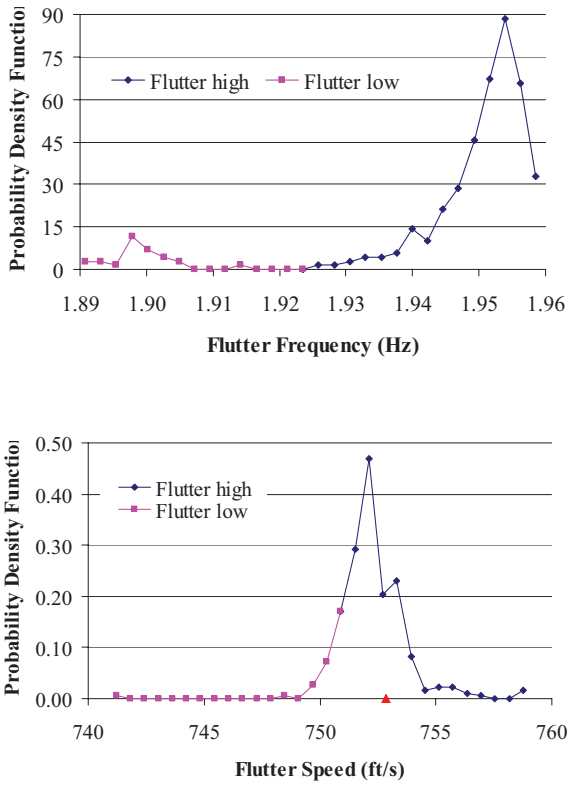

Figure 11. Probability density functions of (a) the flutter frequency and (b) the flutter speed, random boundary conditions. The red triangle denotes the design conditions (fully clamped wing).

UNCERTAIN COUPLING BETWEEN SUBSTRUCTURES

The modeling procedure described above can be extended to the consideration of uncertainty in the coupling between substructures such as the wing of Fig. 12 For simplicity, assume that there are only two substructures the dynamics of which will be represented by two sets of mode shapes, $\underline{\underline{\Phi}}_1$ and $\underline{\underline{\Phi}}_2$, and two sets of constraints modes, $\underline{\underline{\Xi}}_1$ and $\underline{\underline{\Xi}}_2$. In Fig. 12, the modes contained in $\underline{\underline{\Phi}}_1$ would correspond to the inboard wing clamped at both its root and the interface with the outboard one. Similarly, the modes in $\underline{\underline{\Phi}}_2$ would correspond to the outboard wing clamped at its interface with the inboard. The constraints modes, $\underline{\underline{\Xi}}_1$ and $\underline{\underline{\Xi}}_2$, are associated solely with the interface. Next, denote by $\underline{q}_i$ and $\underline{Y}_i$, i = 1,2, the generalized

coordinates associated with the modes and constraint modes of the two substructures. Paralleling the above developments, an expansion of the variables $\underline{Y}_i$ will further be sought as

$$\underline{Y}_i = \underline{\underline{\Psi}}_i \, \underline{u}_i \qquad i = 1,2 \qquad (28)$$

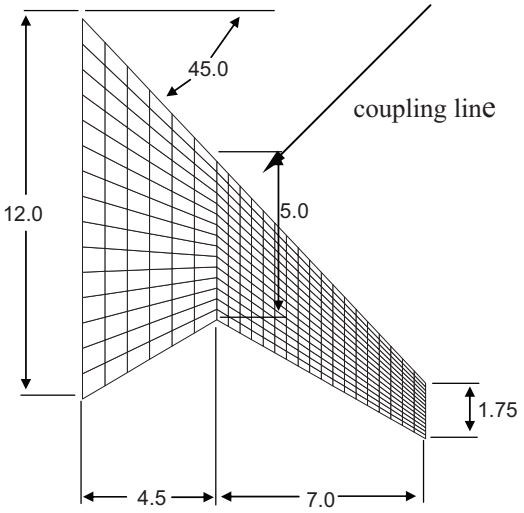

Figure 12. Wing example definition (dimensions in feet)

where $\underline{\underline{\Psi}}_i$ denote the eigenvector matrices of the boundary modes obtained as in Eq. (19). This process will then lead to the overall reduced order model of the structure with *flexible* coupling between its substructures. Specifically, for the reduced order model variables

$$\underline{X}_{ROM} = \left[\underline{q}_1^T \quad \underline{u}_1^T \quad \underline{q}_2^T \quad \underline{u}_2^T \right]^T \qquad (29)$$

it is found that the overall stiffness and mass matrices are

$$\underline{\underline{K}}_{ROM} = \begin{bmatrix} \overline{\underline{\underline{K}}}^{q_1 q_1}_{ROM} & \overline{\underline{\underline{K}}}^{q_1 u_1}_{ROM} & & \\ \overline{\underline{\underline{K}}}^{u_1 q_1}_{ROM} & \overline{\underline{\underline{K}}}^{u_1 u_1}_{ROM} + k\, \hat{\underline{\underline{K}}}^{u_1 u_1}_{ROM} & & -k\, \hat{\underline{\underline{K}}}^{u_1 u_2}_{ROM} \\ & & \overline{\underline{\underline{K}}}^{q_2 q_2}_{ROM} & \overline{\underline{\underline{K}}}^{q_2 u_2}_{ROM} \\ & -k\, \hat{\underline{\underline{K}}}^{u_2 u_1}_{ROM} & \overline{\underline{\underline{K}}}^{u_2 q_2}_{ROM} & \overline{\underline{\underline{K}}}^{u_2 u_2}_{ROM} + k\, \hat{\underline{\underline{K}}}^{u_2 u_2}_{ROM} \end{bmatrix} \qquad (30)$$

and

$$\overline{\underline{\underline{M}}}_{ROM} = \begin{bmatrix} \overline{\underline{\underline{M}}}^{q_1 q_1}_{ROM} & \overline{\underline{\underline{M}}}^{q_1 u_1}_{ROM} & & \\ \overline{\underline{\underline{M}}}^{u_1 q_1}_{ROM} & \overline{\underline{\underline{M}}}^{u_1 u_1}_{ROM} & & \\ & & \overline{\underline{\underline{M}}}^{q_2 q_2}_{ROM} & \overline{\underline{\underline{M}}}^{q_2 u_2}_{ROM} \\ & & \overline{\underline{\underline{M}}}^{u_2 q_2}_{ROM} & \overline{\underline{\underline{M}}}^{u_2 u_2}_{ROM} \end{bmatrix} . \qquad (31)$$

with notations consistent with those introduced in connection with the treatment of uncertain boundary conditions. It remains to specify the coupling stiffness matrix $\hat{\underline{\underline{K}}}_{phys}$ joining the two sets of constraint modes displacements. In parallel with the discussion of the previous section, it is assumed here that

$$\hat{\underline{\underline{K}}}_{phys} = k \left[\overline{\underline{\underline{K}}}^{B_1 B_1}_{phys} + \overline{\underline{\underline{K}}}^{B_2 B_2}_{phys} \right] \qquad (32)$$

where the notation B_iB_i is introduced here to specify the side of the common boundary (i.e. substructure *i*). Then, as in Eq. (23), one obtains

$$\hat{\underline{\underline{K}}}^{u_i u_j}_{ROM} = \underline{\underline{\Psi}}_i^T \, k \left[\overline{\underline{\underline{K}}}^{B_1 B_1}_{phys} + \overline{\underline{\underline{K}}}^{B_2 B_2}_{phys} \right] \underline{\underline{\Psi}}_j \, . \qquad (33)$$

This approach has been demonstrated on the wing of Fig. 12. Given the small number of nodes at the interface and the observed slow convergence with the number of boundary modes, all such modes were kept here and 20 clamped modes were taken for each substructure. Shown in Fig. 13 is the convergence, as *k* increases, of the first natural frequency of the system to the corresponding value for the single cantilevered structure. The next 6 natural frequencies were found to converge faster than the first one.

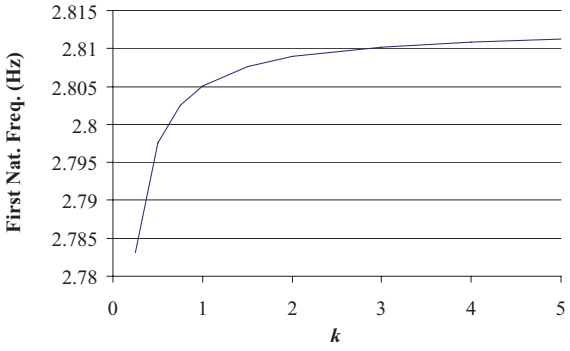

Figure 13. Convergence of the first natural frequency of the assembled wing as *k* increases.

The effects of varying the parameters *k* and δ were again assessed on the coefficient of variation of the natural frequencies and on the boundary energy. The results, see Figs 14 and 15, are consistent with those obtained for the boundary condition uncertainty, see Figs 7 and 8.

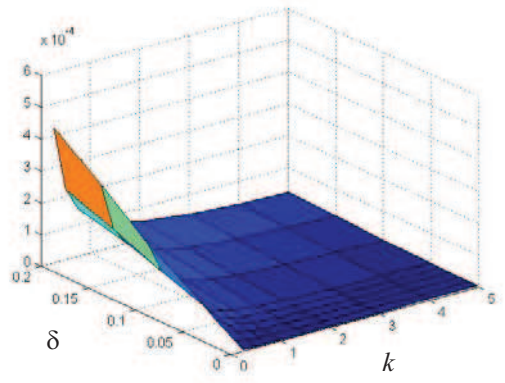

First natural frequency

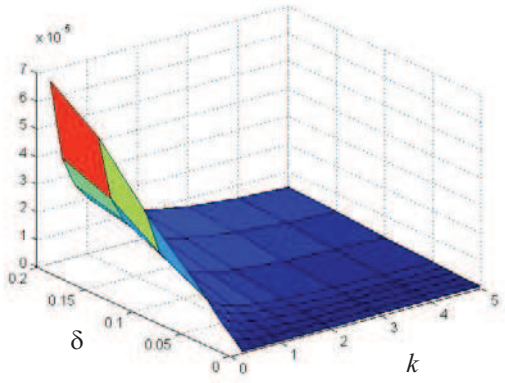

Second natural frequency

Figure 14. Coefficients of variation of the first two natural frequency vs. k and δ, all boundary modes, 20 clamped modes each substructure, wing example.

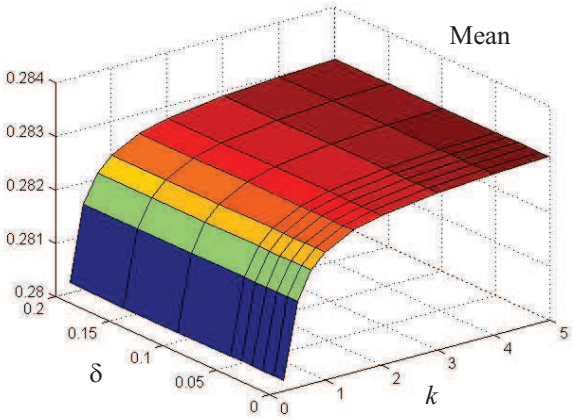

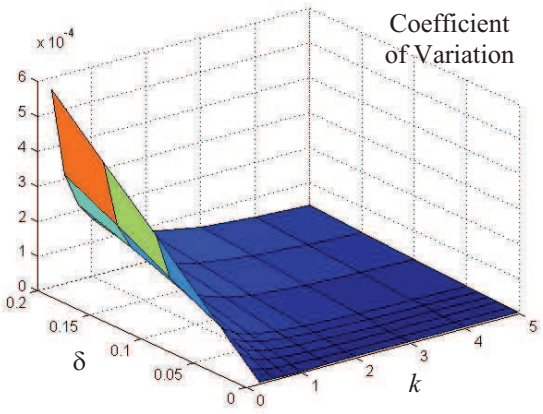

Figure 15. Mean and coefficient of variation of E_{BC}, first mode deformations, vs. k and δ, all boundary modes, 20 clamped modes each substructure, wing example.

SUMMARY

The focus of this investigation was on the formulation and validation of a novel approach for the inclusion of uncertainty in the modeling of the boundary conditions of linear structures and of the coupling between linear substructures. The three steps of the approach are: (i) the determination of a mean structural dynamic model including boundary condition/coupling flexibility, (ii) the introduction of uncertainty in the mean model, and (iii) the estimation of the mean and uncertainty parameters of the model.

A Craig-Bampton substructuring approach was adopted for the formulation of the mean model with boundary condition/coupling flexibility. This flexibility was implemented through the finite stiffness matrix $\underline{\underline{\hat{K}}}^{BB}_{phys}$, see Fig. 2 and Eq. (23). Note in this regard that the ensuing consideration of model uncertainty (in addition to parameter uncertainty) does render less critical the detailed representation of $\underline{\underline{\hat{K}}}^{BB}_{phys}$ and thus validates the straightforward assumption of Eq. (23).

The simulation of uncertainty was addressed using the nonparametric stochastic modeling approach first because it includes model and parameter uncertainties, both of which are expected to be present, but also because of its computational convenience. Indeed, random matrices $k\underline{\underline{K}}^{uu}_{ROM}$ are readily generated using the algorithm of Eqs (2)-(5) or Fig. 1.

Each of the above step, i.e. the mean model construction and the nonparametric approach,

introduces one parameter in the problem, i.e. k for the mean model and δ for the uncertainty characterization. The estimation of these parameters could be performed from global variables, e.g. from the mean and standard deviation of the first natural frequency, but they might then be affected by the presence of uncertainty on other aspects of the structure (other boundary/coupling, uncertain material/geometrical properties, etc.) Accordingly, it was proposed here to estimate k and δ using measurements performed on the uncertain boundary. In fact, the value of k was readily shown to correlate very strongly with the mean energy on the boundary, see Eq. (27), while δ exhibited a similar relationship with the standard deviation of this energy.

The consideration of uncertainty in the coupling between substructures was formulated in a similar manner to that of the boundary conditions through a Craig-Bampton modeling approach of all connecting substructures.

Finally, these developments permitted the flutter analysis of wings with uncertain boundary condition or uncertain coupling between substructures. It was observed in particular that the resulting level of uncertainty on the flutter boundary was significantly larger than on the natural frequencies and thus is of practical interest.

REFERENCES

[1] Soize, C., 2000, "A Nonparametric Model of Random Uncertainties on Reduced Matrix Model in Structural Dynamics," *Probabilistic Engineering Mechanics*, Vol. 15, No. 3, pp. 277-294.

[2] Soize, C., 2001, "Maximum Entropy Approach for Modeling Random Uncertainties in Transient Elastodynamics," *Journal of the Acoustical Society of America*, Vol. 109, No. 5, pp. 1979-1996.

[3] Soize, C., 2005, "Random Matrix Theory for Modeling Uncertainties in Computational Mechanics," *Computer Methods in Applied Mechanics and Engineering*, Vol. 194, pp. 1333-1366.

[4] Mignolet, M.P., and Soize, C., 2006, "Nonparametric Stochastic Modeling of Linear Systems with Prescribed Variance Information of Several Natural Frequencies," *Proceeding of the Fifth International Conference on Computational Stochastic Mechanics*, Rhodes, Greece, Jun. 21-23. To appear in *Probabilistic Engineering Mechanics*. 2008.

[5] Kim, K., Kim, Y.C., Mignolet, M.P., Liu, D.D., Chen, P.C., Lee, D.H., "Random Aeroelastic Response Due to Strong Hypersonic Unsteady-Wave/Shock Interaction with Acoustic Loads," *Proceedings of the 48th Structures, Structural Dynamics, and Materials Conference*, Honolulu, Hawaii, Apr. 23-26, 2007. AIAA Paper AIAA-2007-2014.

[6] Mignolet, M.P., and Chen, P.C., "Aeroelastic Analyses with Uncertainty in Structural Properties," *Proceeding of the AVT-147 Symposium: Computational Uncertainty in Military Vehicle Design*, Athens, Greece, Dec. 3-7, 2007.